Radiation Measurements 177 (2024) 107261

Contents lists available at ScienceDirect

Radiation Measurements

journal homepage: www.elsevier.com/locate/radmeas

Exploring the luminescence properties and dosimetric characteristics of $CaSO_4$:Tb, $CaSO_4$:Mn, and $CaSO_4$:Mn,Tb phosphors synthesized by slow evaporation route

Anderson M.B. Silva [a,b,*], Daniel S. Rodrigues [b], Beatriz D.O. Guedes [b], Iury S. Silveira [a], Patrícia L. Antonio [a], Danilo O. Junot [c], Linda V.E. Caldas [a], Divanizia N. Souza [b]

[a] Instituto de Pesquisas Energéticas e Nucleares, Comissão Nacional de Energia Nuclear, IPEN/CNEN-SP, Av. Prof. Lineu Preste, 2242, 05508-000, São Paulo, SP, Brazil
[b] Departamento de Física, Universidade Federal de Sergipe, Marechal Rondon, S/N, 49100-000, São Cristovão, SE, Brazil
[c] Instituto de Física Armando Dias Tavares, Universidade do Estado do Rio de Janeiro, UERJ, Rua São Francisco Xavier, 524, 20550-013, Rio de Janeiro, RJ, Brazil

ARTICLE INFO

Keywords:
$CaSO_4$
Dosimetry
Thermoluminescence
Optically stimulated luminescence
Structure properties
And optical properties

ABSTRACT

This work aimed to investigate and compare the luminescence properties of $CaSO_4$:Tb, $CaSO_4$:Mn, and $CaSO_4$:Mn,Tb synthesized by slow evaporation route. The crystalline structure, morphology, and optical properties of the phosphors were characterized by X-ray diffraction analysis (XRD), photoluminescence (PL), radioluminescence (RL), and scanning electron microscopy (SEM). In addition, thermoluminescence (TL) and optically stimulated luminescence (OSL) were used to comprehensively investigate the dosimetric properties of the phosphors, such as the TL glow curve and continuous wave OSL (CW-OSL) curves, dose-response and its reproducibility, fading, and sensitivity. For dosimetric analyses, the samples were irradiated with beta radiation. PL and RL emission spectra confirmed the presence of Tb^{3+} and Mn^{2+} ions in crystalline matrices. The samples showed a typical exponential OSL decay curve, indicating that the charge traps have a high photoionization cross-section for blue LEDs. The synthesized pellets exhibited good luminescent and dosimetric properties, with linear luminescent response over a wide dose range (169 mGy–100 Gy) and reproducibility of both OSL and TL signals. Furthermore, the incorporation of terbium as a co-dopant in the $CaSO_4$:Mn matrix reduced its fading from 75% to only 17%. The phosphors had high TL and OSL sensitivities in comparison to some commercially available dosimeters.

1. Introduction

Interest in solid-state luminescence spans various scientific domains, such as atomic/molecular spectroscopy, structural material analysis, and crystal lattice defects. This phenomenon offers a precise method for measuring radiation exposure, ensuring reliable experimental results for environmental, personal, clinical, retrospective accident analysis, and industrial applications (Bakr et al., 2020; Guckan et al., 2017; Haninger et al., 2016; Pradhan et al., 2008; Yasmin et al., 2020).

Luminescent materials, categorized into scintillators and dosimeters, play a pivotal role in ionizing radiation detection (Nakauchi et al., 2016). Scintillators which promptly convert ionizing radiation into visible photons upon absorption are applied in various fields, such as medical imaging, security, astrophysics, and geophysical exploration (Marzougui and Hassen-Chehimi, 2019; Totsuka et al., 2011; Yanagida et al., 2010). In contrast, dosimeters serve a distinctly different yet equally vital function in radiation monitoring. Unlike scintillators, dosimeters accumulate the energy deposited by incident radiation over time, offering a cumulative measure of exposure. This accumulated energy is subsequently released as light when the dosimeter is exposed to external factors.

Thermoluminescence (TL) and optically stimulated luminescence (OSL) techniques exploit the phosphorescent emission of a previously irradiated and stimulated material. TL involves stimulating the material using heat, whereas OSL utilizes photons within a specific wavelength range as the stimulus. The light emitted from the material is proportional to the absorbed radiation dose (McKeever et al., 1995)

Luminescent materials efficiently capture absorbed energy through

* Corresponding authorInstituto de Pesquisas Energéticas e Nucleares, Comissão Nacional de Energia Nuclear, IPEN/CNEN-SP, Av. Prof. Lineu Preste, 2242, 05508-000, São Paulo, SP, Brazil
E-mail address: andersonmanoel22@hotmail.com (A.M.B. Silva).

https://doi.org/10.1016/j.radmeas.2024.107261
Received 20 February 2024; Received in revised form 26 July 2024; Accepted 29 July 2024
Available online 30 July 2024

carrier trapping, leading to re-excitation and recombination of carriers that generate measurable luminescence. Current research efforts address a wide range of materials, from powders, chips, fibers, and thin films to ceramics, glasses, and single crystals, with the goal of improving dosimetry techniques (Chen and McKeever, 1997; Junot et al., 2019; Yasmin et al., 2020).

The dosimetry principle is based on the proportional relationship between TL/OSL intensity and electron-hole pair recombination, which is representative of the dose absorbed by the dosimeter. The meticulous design of materials to optimize electron and hole trapping is crucial for the increased sensitivity of luminescent materials and for achieving greater accuracy in ionizing radiation measurements (McKeever, 2022).

Since the first successful application of LiF and SrS-based materials in dosimetry (Antonov-Romanovskii et al., 1955; Daniels et al., 1953), several materials, including $CaSO_4$, have been proposed for solid-state dosimetry. The first investigated synthetic material used as a TL dosimeter, $CaSO_4$:Mn, exhibits high sensitivity but significant fading of its TL signal, thus limiting its application (Watanabe, 1951). Common $CaSO_4$-based Thermoluminescent Dosimeters (TLDs) in routine dosimetry, doped with dysprosium or thulium, have a wide linear response range to ionizing radiation doses (Lakshmanan, 1999).

Recent studies have improved the luminescent properties of $CaSO_4$ by adding rare earth and metal elements as dopants and co-dopants, making this compound one of the most sensitive thermoluminescent materials. Various dopants and co-dopants have been explored to enhance its performance (Doull et al., 2014; Guckan et al., 2017, 2019, 2023; Junot et al., 2011, 2014, 2016, 2019, 2020; Kása et al., 2007; Silva et al., 2020, 2022; Yukihara et al., 2014, 2015).

As a result, various methods have been employed for the preparation of $CaSO_4$ crystals, such as the co-precipitation method (Guckan et al., 2017; Khan et al., 2015), the recrystallization method (Bahl et al., 2017), the hydrothermal method (Zahedifar et al., 2011), the sol-gel method (Kadari et al., 2016), the solid-state reaction route (Rani et al., 2015), and the slow evaporation route (Yamashita et al., 1970).

Therefore, based on the presented background information, we employed the Yamashita method (Yamashita et al., 1970) in our study for the preparation of $CaSO_4$ crystals. This method, characterized by its slow evaporation approach, underwent specific modifications in the production process. These adjustments resulted in a crystal growth system with a controlled air atmosphere and an improved distillation system, fully isolated from the external environment, thereby facilitating the reuse of sulfuric acid in the phosphor production process. These refinements were inspired by the contributions of Junot et al. (2016). The applied method ensures more precise conditions for crystal growth, potentially resulting in phosphors of higher quality and purity compared to conventional techniques. Additionally, complete isolation from external environmental factors reduces the risk of contamination of the crystals during their synthesis, enhancing reliability and reproducibility.

Considering the importance of maintaining dosimetric studies on $CaSO_4$-based phosphors through this method, and with the aim of developing a material to be used as a TL/OSL dosimeter, this research focuses on the production of $CaSO_4$:Tb, $CaSO_4$:Mn, and $CaSO_4$:Mn,Tb phosphors, as well as the characterization of their structural, optical, and dosimetric properties. The new materials are intended to serve as alternative dosimeters to those which are currently available.

It is expected that the results of this study will contribute to the consolidation and expansion of the knowledge regarding these materials. This investigation is part of a continuous experimental series initiated by our research group, building on the fundamental findings of previous studies by Junot et al. (2011, 2014, 2016, 2019, 2020). These earlier works established the viability of the slow evaporation route for producing doped $CaSO_4$ crystals, including variants such as $CaSO_4$:Eu, $CaSO_4$:Eu,Ag, $CaSO_4$:Tb,Yb, $CaSO_4$:Tb,Eu, $CaSO_4$:Tm, and $CaSO_4$:Tm, Ag. Additionally, these studies conducted thorough structural, optical, and dosimetric analyses. These studies revealed materials with properties suitable for dosimetric applications, indicating their potential use as TL/OSL dosimeters. Furthermore, the current study builds on the progress made by Silva et al. (2020, 2021, 2022, 2023), who extensively investigated doped and co-doped $CaSO_4$, exploring unconventional ions such as terbium, manganese, and silver. Their initial research efforts significantly enhanced the luminescent properties of these materials, thereby advancing both the understanding of these materials and their potential for further development in the field of radiation dosimetry.

2. Materials and methods

The $CaSO_4$:Tb, $CaSO_4$:Mn, and $CaSO_4$:Mn,Tb crystals were synthesized via a slow evaporation method from a mixture of calcium carbonate (CaCO3) (Merck, 99%), sulfuric acid (H_2SO_4 (Vetec, 95%–99%), terbium oxide (Tb_4O_7) (Alfa Aesar, 99.9%), and manganese nitrate ($Mn(NO_3)_2.4H_2O$) at a concentration of 0.1 mol%. This concentration has been carefully determined through optimization studies designed to maximize the luminescent properties of the crystals, while also maintaining their structural integrity. By maintaining this standardized dopant concentration, our methodology ensures consistency and allows meaningful comparisons between differently doped samples.

The compound production system, in which crystal growth takes place, consists of three parts: a sealed system, an air circulation system, and a heating system. The crystal growth parameters were established based on previous studies (Junot et al., 2016, 2019; Silva et al., 2020).

The evaporation temperature was maintained using a heating mantle at 375 °C until all the acid evaporated (approximately 24 h). Following the evaporation of the sulfuric acid, the crystals were washed, ground, and sieved. The resulting powders were calcined at 600 °C for 1 h. Subsequently, crystals ranging from 75 to 150 μm in grain size were homogeneously blended with polytetrafluoroethylene (Teflon) in a 1:1 ratio to enhance the material's resistance. By applying a uniaxial pressure of 0.5 tons for 10 s, meticulously crafted pellets weighing 40 ± 1 mg, with a diameter of 6 mm and thickness of approximately 1 mm, were produced. Finally, the pellets were sintered at 450 °C for 1 h to improve their strength and enhance the stability of TL/OSL signals.

Powder X-ray diffractograms (XRD) were obtained using a Rigaku diffractometer (RINT, 2000/PC) with Cu-K_α at a generator voltage of 60 kV and a current of 30 mA. This analysis was carried out in continuous scanning mode from 20° to 80° (2θ) with 0.05° (2θ) steps. The XRD patterns were compared with reference data from the International Centre for Diffraction Data (ICDD). The JASCO FP8600 spectrofluorometer was utilized to acquire photoluminescence spectra, capturing both excitation and emission spectra. PL measurements were performed using a 150 W xenon discharge lamp as the excitation source. All measurements were made under identical conditions, and the final spectra represent the average of three measurements for each sample. The measurements were conducted with calcined powder, coupled with the FPA-810 holder attached to the PSH-002 cell model. The fluorescent emission spectra of the produced samples were monitored through radioluminescence. The samples were excited with X-ray radiation (40 kV voltage and 0.2 mA current) from an X-ray tube manufactured by Moxtek at room temperature. Luminescence from the samples was continuously collected by an Ocean Optics fiber optic spectrometer, model USB2000 with collimation lens, with data acquisition facilitated by a computer. Emission spectra were measured in the 200–1000 nm range, with an excitation time of 3 s and an integration time of 20 s. Scanning electron microscope (SEM) images were captured using a Hitachi TM-3000 SEM equipped with a carbon substrate.

The samples were excited with X-ray radiation (40 kV voltage and 0.2 mA current) from an X-ray tube manufactured by Moxtek at room temperature. Luminescence from the samples was continuously collected by an Ocean Optics fiber optic spectrometer, model USB2000 with collimation lens, with data acquisition facilitated by a computer. Emission spectra were measured in the 200–1000 nm range, with an excitation time of 3 s and an integration time of 20 s.

A DA-20 model RisØ TL/OSL reader system was used for TL and OSL measurements. The samples were irradiated with a $^{90}Sr+^{90}Y$ beta source. For TL/OSL detection, the Hoya U-340 was positioned in front of the bialkali photomultiplier tube (PMT) unit. In TL measurements, a heating rate of 10 °C/s was used, reaching a maximum temperature of 400 °C. During OSL measurements, the signal was collected over 40 s and the samples were stimulated with blue LEDs, which emitted light at a wavelength of 470 nm and operated in continuous-wave mode. Although high heating rates can lead to thermal lag and shifts in peak temperatures, such rates are commonly selected for practical dosimetry applications (Fernández et al., 2016). This limitation is crucial to acknowledge to ensure the acquisition of comparable and reproducible data across different investigations, thereby making our findings relevant and applicable in the broader scientific community.

To assess the peaks in the TL emission curves, the $T_m \times T_{stop}$ technique was used. For each type of sample, 15 pellets were selected based on reproducibility tests, and three pellets used in each temperature interval. Each pellet was first preheated to a given temperature (T_{stop}) at a heating rate of 10 °C/s using the Risø TL/OSL reader heating system. After cooling down to room temperature, the pellet was reheated at at the same heating rate for the TL reading to a final temperature of 400 °C. The average temperature of the lowest temperature peak observed (T_m) was evaluated.

For the TL sensitivity analysis, we performed a comparison between five commercial dosimeters and the $CaSO_4$:Mn, $CaSO_4$:Mn,Tb, and $CaSO_4$:Tb phosphors. The dosimeters were $CaSO_4$:Dy (the Harshaw TLD-900), LiF:Mg,Ti (the Harshaw TLD-100), CaF_2:Dy (the Harshaw TLD-200), CaF_2:Mn (the Harshaw TLD-400), Al_2O_3:C (Rexon™), and $CaSO_4$:Dy (the Harshaw TLD-900). All the pellets were pre-irradiated with a beta source up to 1 Gy. The glow curves were then immediately read through a Hoya U-340 (340 ± 40 nm) filter. After each TL and OSL evaluation, the pellets were placed on aluminum plates for reusability purposes and thermally treated at 400 °C for 60 min in a 671 IRD/CNEN furnace.

3. Results and discussions

3.1. Structural characterization

The crystal structure of the synthesized powders was checked by XRD measurements. In Fig. 1, it can be seen that the measured diffraction patterns correlate to the reference pattern (ICDD 00-037-1496). The variations in intensities in the diffractograms are associated with the influence of different dopants incorporated during the synthesis process. These variations, in addition to confirming the controlled introduction of impurities, suggest a possible modification in the diffracted intensity, indicating potential changes in the crystal structure.

In all diffractograms (Fig. 1), the Bragg peaks can be easily identified, indicating the absence of secondary phases in the samples. The interplanar distances, d_{hkl}, of the five main peaks at 25.25°, 31.25°, 38.55°, 40.70°, and 48.65° were determined to be 3.524 Å, 2.859 Å, 2.333 Å, 2.215 Å, and 1.870 Å, respectively. These peaks correspond to the (020), (012), (202), (212), and (032) reflection planes. The lattice parameters of the samples were calculated using the established formula for the orthorhombic structure (Dasa et al., 2016). These results demonstrate the consistency of the crystal structures of the samples with the ICDD 00-037-1496 standard, which has lattice parameters of a = 6.993 Å, b = 7.001 Å, and c = 6.241 Å.

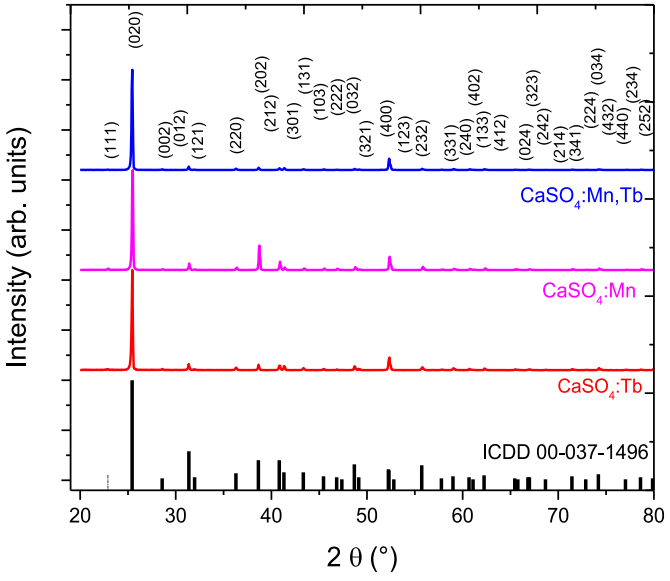

Fig. 1. X-ray diffractograms of $CaSO_4$:Tb, $CaSO_4$:Mn, and $CaSO_4$:Mn,Tb powders, presented alongside the crystallographic standard (ICDD 00-037-1496) and standard Bragg reflections.

3.2. Photoluminescence studies

Fig. 2 presents the excitation spectra of Tb^3 doped compounds, with emission monitored at the $^5D_4 \rightarrow {}^7F_5$ transition at 545 nm. The excitation spectra of the phosphors exhibit a peak at 213 nm, attributed to the 4f-5d electronic transition of Tb^{3+}, along with a weak absorption band ranging from 240 to 400 nm corresponding to 4f-4f transitions (Li et al., 2017).

The emission spectra were obtained with excitation monitored in the higher-energy band (related to the 4f-5d transitions) at 213 nm. The emissions consist of $4f_8 \rightarrow 4f_8$ transitions in the green and blue regions. The green emissions are attributed to the $^5D_4 \rightarrow {}^7F_J$ (J = 6, 5, 4, and 3) transitions, while the blue emissions are attributed to the $^5D_3 \rightarrow {}^7F_J$ (J = 5, 4, 3, and 2) transitions (Hao et al., 2009; Li et al., 2017). The excitation and emission spectra of $CaSO_4$:Tb and $CaSO_4$:Mn,Tb exhibit a similar profile, with an increased intensity in the samples co-doped with Mn^{2+}. This enhancement is attributed to increased absorption and energy transfer from the host to the Tb^{3+} ions in the presence of Mn^{2+}, and therefore co-doping with Mn^{2+} proved to be more effective in creating structural defects in the $CaSO_4$ matrix.

Fig. 3 displays excitation spectra with emission monitored at 493 nm. The $CaSO_4$:Mn,Tb spectrum exhibits peaks with a maximum at 213 nm and a weak absorption band from 240 to 400 nm. These were also observed when the samples were excited at 545 nm, as discussed earlier,

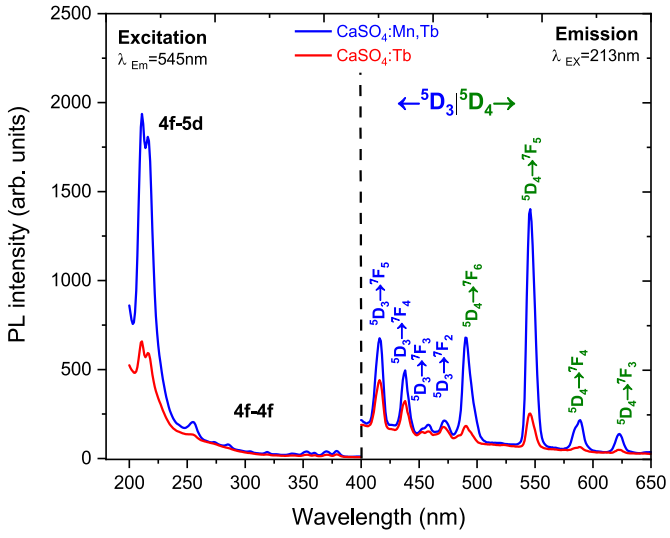

Fig. 2. The emission and excitation spectra of $CaSO_4$:Tb and $CaSO_4$:Mn,Tb samples, highlighting the Tb^{3+} transition (λ_{exc} = 213 nm, λ_{em} = 545 nm).

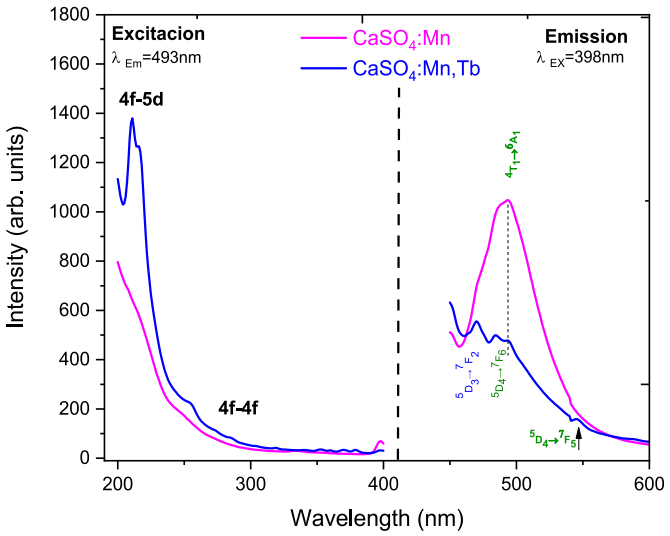

Fig. 3. The emission and excitation spectra of $CaSO_4$:Mn and $CaSO_4$:Mn,Tb samples, showing the Mn^{2+} transition (λ_{exc} = 398 nm, λ_{em} = 493 nm).

and were attributed to the 4f-5d and 4f-4f transitions of Tb^{3+} ions, respectively. Meanwhile, the excitation spectrum of $CaSO_4$:Mn shows a band starting at 200 nm, which is attributed to the excitation of the $(SO_4)^{2-}$ complex (Van der Kolk et al., 2001). Additionally, a characteristic band at 398 nm is observed and is assigned to the $^6A_1(^6S) \rightarrow {}^4T_2(^4D)$ transitions of Mn^{2+} ions (Hou et al., 2012).

Moving onto the emission spectra monitored at 398 nm. The green emission region at ~500 nm is typical for bivalent manganese ions, corresponding to the $^4T_1 \rightarrow {}^6A_1$ transition of the Mn^{2+} ion (Luchechko et al., 2019; Menon et al., 2005; Zahedifar et al., 2011). Other emissions observed in the $CaSO_4$:Mn,Tb spectrum at 470 nm ($^5D_3 \rightarrow {}^7F_2$), 490 nm ($^5D_4 \rightarrow {}^7F_6$), and 544 nm ($^5D_4 \rightarrow {}^7F_5$) correspond to Tb^{3+} ion transitions (Hao et al., 2009; Li et al., 2017). The appearance of Tb^{3+} absorption bands confirms that Mn^{2+} ions are essentially excited by Tb^{3+} ions because the emission at around 490 nm is only observed in the Mn^{2+} spectrum, resulting in an energy transfer from Tb^{3+} ions to Mn^{2+} ions. According to the energy transfer theory developed by Dexter (1953), the energy transfer mechanism based on multipolar interaction depends on the overlap of the emission spectrum of the sensitizer (Tb^{3+}) with the absorption spectrum of the acceptor (Mn^{2+}). Therefore, the energy transfer process from Tb^{3+} ions to Mn^{2+} ions depends on the degree of overlap between the emission band of Tb^{3+} and the absorption band of Mn^{2+}. Due to the partial overlap of the emission bands of the $^5D_4$ levels with the absorption band of the $^4T_1$ level, it is reasonable to assume that the energy transfer process may be associated with the $^4T_1$ level of Mn^{2+}. Thus, the energy transfer process can be described as follows: the energy that populates the $^5D_4$ level through nonradiative relaxation from higher energy levels or direct absorption is transferred to the $^4T_1$ levels through the multipolar interaction. Characteristic luminescence occurs as a result of this process (You et al., 2008).

3.3. Radioluminescence studies

Fig. 4 presents the RL emission spectra of $CaSO_4$:Tb, $CaSO_4$:Mn, and $CaSO_4$:Mn,Tb samples excited by X-rays. The presence of Tb^{3+} ions in the doped samples is evidenced by the radioluminescence bands, ranging from violet to red. The $^5D_3 \rightarrow {}^7F_J$ (J = 6–2) and $^5D_4 \rightarrow {}^7F_J$ (J = 6–3) transitions are responsible for the nine typical lines of Tb^{3+}, with a peak intensity at ~546 nm (transition $^5D_4 \rightarrow {}^7F_5$). It is observed that in the violet and blue region (380–480 nm), the emissions from $CaSO_4$:Tb are less intense compared to those from $CaSO_4$:Mn,Tb (Fig. 4a). This reduction in luminescent intensity can be attributed to the energy transfer mechanism related to the multipolar interaction of the $^4T_1$ level of Mn^{2+} ions. The overlap of the Tb^{3+} emission band with the Mn^{2+} absorption band contributes to an increase in the intensity of the $^5D_4 \rightarrow {}^7F_6$ transition. The emissions of mono-doped manganese samples are dominated by a green emission band at around 494 nm, which is associated with the $^4T_1(^4G) \rightarrow {}^6A_1(^6S)$ transition of Mn^{2+} ions (Fig. 4b).

3.4. Scanning electron microscopy

Micrographs of the surfaces of the phosphorus pellets were obtained at different magnifications to analyze the grain behavior after pressing and sintering. Fig. 5a displays a micrograph showing a homogeneous and cohesive surface of one of the $CaSO_4$:Mn,Tb pellets. At a higher magnification, Fig. 5b highlights the low porosity of the pellets. This low porosity is achieved through factors such as crystal selection, the use of Teflon (DuPont) as a binder, controlled pressure during material compaction, and precise sintering temperatures. Low porosity is crucial for dosimetric applications because it improves thermal conductivity, prevents moisture and contaminants ingress, contributes to uniform radiation absorption distribution, and facilitates pellet reuse. This characteristic of the samples helps maintain the consistency of the

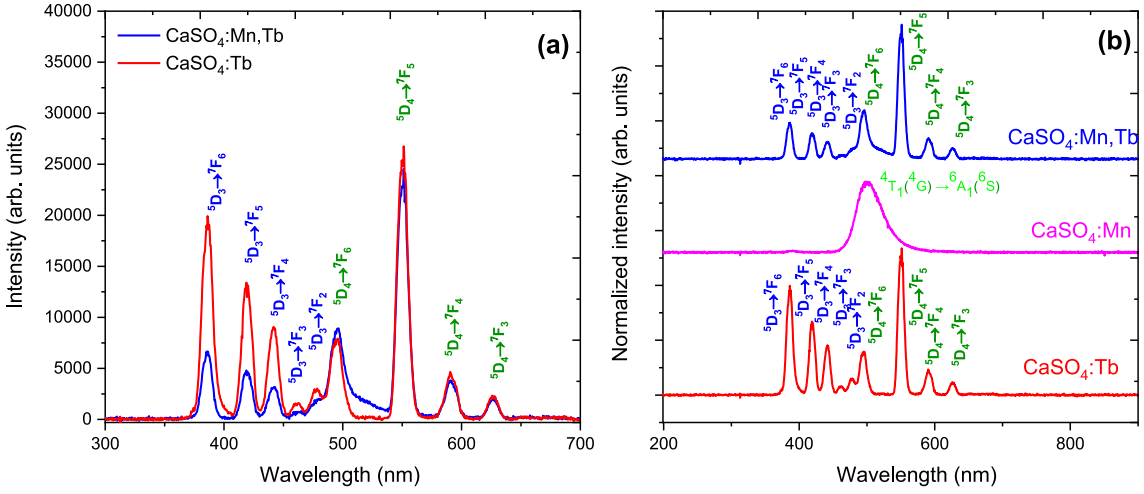

Fig. 4. Radioluminescence of (a) $CaSO_4$:Tb and $CaSO_4$:Mn,Tb samples and (b) $CaSO_4$:Tb, $CaSO_4$:Mn, and $CaSO_4$:Mn,Tb samples under X-ray excitation.

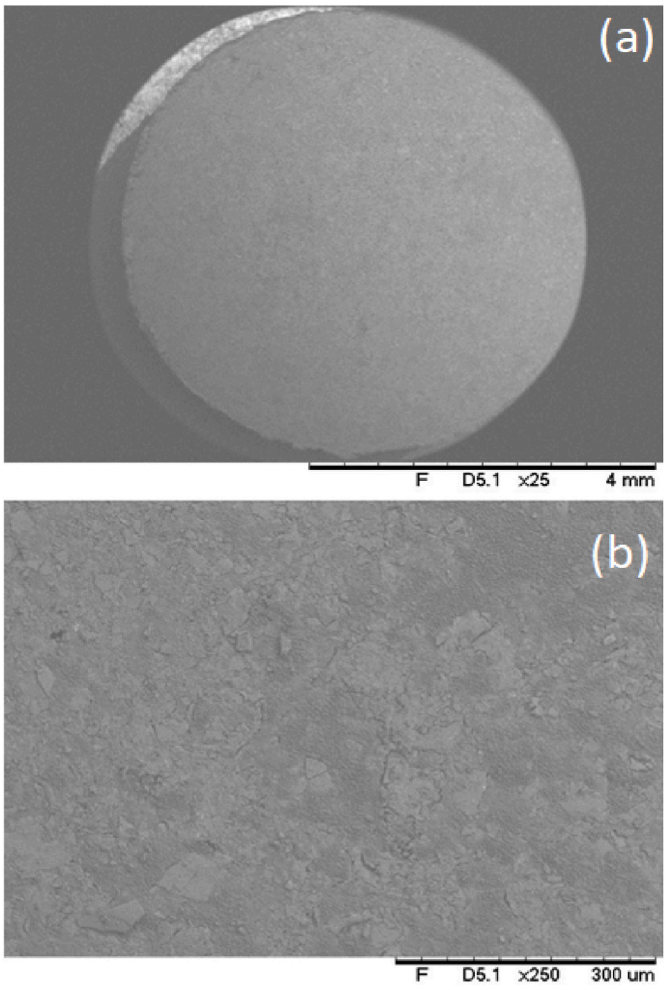

Fig. 5. SEM micrograph of one of the $CaSO_4$:Mn,Tb pellets produced after sintering at 450 °C for 1 h at approximate magnifications of (a) 25 × and (b) 250 × .

emitted luminescence signal and prevents grain breakage and detachment.

3.5. Thermoluminescence studies

3.5.1. Thermoluminescence glow curve

TL emission curves were obtained for the $CaSO_4$:Tb, $CaSO_4$:Mn, and $CaSO_4$:Mn,Tb compounds. As shown in Fig. 6, $CaSO_4$:Mn exhibited the most intense TL emission curve, followed by $CaSO_4$:Mn,Tb, and then $CaSO_4$:Tb. $CaSO_4$:Mn displayed a TL peak centered at 190 °C for a heating rate of 10 °C/s. It is crucial to acknowledge that variations in TL emission curves can stem from diverse factors, including synthesis method and measurement conditions, such as the heating rate. Comparisons with results from other studies (Medlin, 1961; Zahedifar et al., 2011) underscore the significance of these influences. For instance, Medlin (1961), via the precipitation method, synthesized $CaSO_4$:Mn samples that emit a single peak at approximately 140 °C. Conversely, Zahedifar et al. (2011) employed the hydrothermal method, resulting in samples with a TL emission curve with three overlapping peaks. Similarly, Yamashita et al. (1970) found that the $CaSO_4$:Mn emission curve exhibited a single peak at 100 °C.

The studied $CaSO_4$:Tb sample presented a primary peak centered at 185 °C and a lower intensity peak at approximately 300 °C. Its TL emission curve resembled that of the co-precipitation-produced compound in the work of Khan et al. (2015). Comparing the TL emission curves of $CaSO_4$:Mn and $CaSO_4$:Mn,Tb, it can be seen that terbium co-doping reduced the peak intensity at 200 °C and introduced a new peak at a higher temperature. This indicates that terbium co-doping introduced new deep trapping centers, distinct from those in $CaSO_4$:Mn.

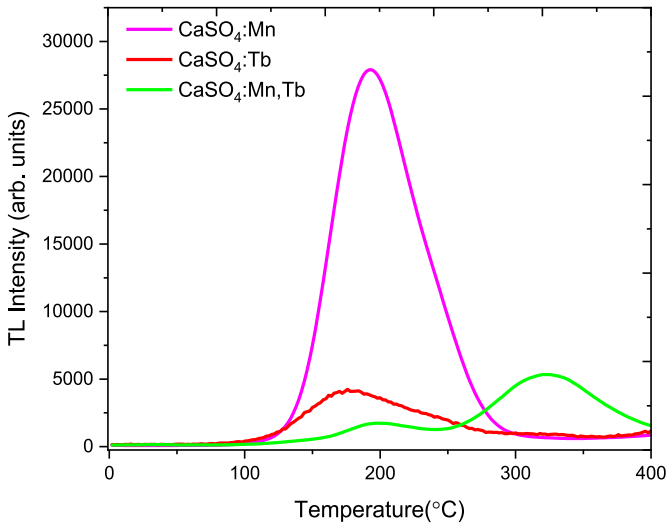

Fig. 6. TL emission curves of $CaSO_4$:Tb, $CaSO_4$:Mn, and $CaSO_4$:Mn,Tb samples irradiated with 1 Gy of beta radiation. A heating rate of 10 °C/s was used for the measurement.

The TL emission curve of $CaSO_4$:Mn,Tb displayed two dosimetric peaks centered at 205 and 325 °C. These peaks are considered "dosimetric" as they lie within a temperature range of 200–300 °C, which is optimal for accurate TL/OSL dosimetry. Minimal undesired charge carrier release at these temperatures increases the accuracy and reliability of radiation dose measurements.

In the study by Menon et al. (2005), an increase in the TL peak intensity of $CaSO_4$:Pr^{3+}, Y^{3+}, and Nd^{3+} was observed due to the addition of Mn^{2+}. In that study, trivalent ions (Pr, Y, and Nd) provided the trapping sites. During irradiation, electrons and holes are trapped, and their recombination during heating excites the Mn^{2+} ions, which then emit TL upon de-excitation. This observation parallels the present study, where we also investigate the TL emission properties of $CaSO_4$ compounds doped with Mn, Tb, and their combinations. However, a similar enhancement in TL is not observed with Mn^{2+} as a co-dopant in the cases of $CaSO_4$:Dy or $CaSO_4$:Tm because the host lattice is already efficient in accommodating these ions.

The $T_m \times T_{stop}$ method of McKeever (1988) was used to evaluate individual peaks in the TL emission curves of the samples irradiated with 1 Gy of beta radiation, where T_m is the peak temperature and T_{stop} is the preheating temperature. Fig. 7 shows well-separated TL peaks within the temperature range studied. According to McKeever, step-like structures (plateaus) in the $T_m \times T_{stop}$ plot indicate well-separated peaks, while a continuous distribution suggests a complex TL peak. For $CaSO_4$:Tb (Fig. 7a), the $T_m \times T_{stop}$ graph shows three distinct peaks at approximately 180, 210, and 270 °C. The first and second plateaus correspond to well-defined traps, while the third peak indicates a continuous distribution. Unlike the T_{stop} region corresponding to the first two peaks, this third region does not have a well-defined plateau and shows a sharp increase in T_m towards higher temperatures.

The $T_m \times T_{stop}$ plot of $CaSO_4$:Mn (Fig. 7b) shows two plateaus attributed to TL peaks at 184 and 219 °C. For $CaSO_4$:Mn,Tb (Fig. 7c), the plateau is observed between 205 and 325 °C, while above 350 °C an overlap of several peaks is apparent. This latter observation is limited because of the reader parameters for TL emission curve acquisition, including sample heating which only extended up to 400 °C.

The TL curve was deconvoluted using the kinetic order equation of Chen and McKeever (1997). As shown in Fig. 8, the $CaSO_4$:Tb samples exhibited an emission curve consisting of an overlap of two intense

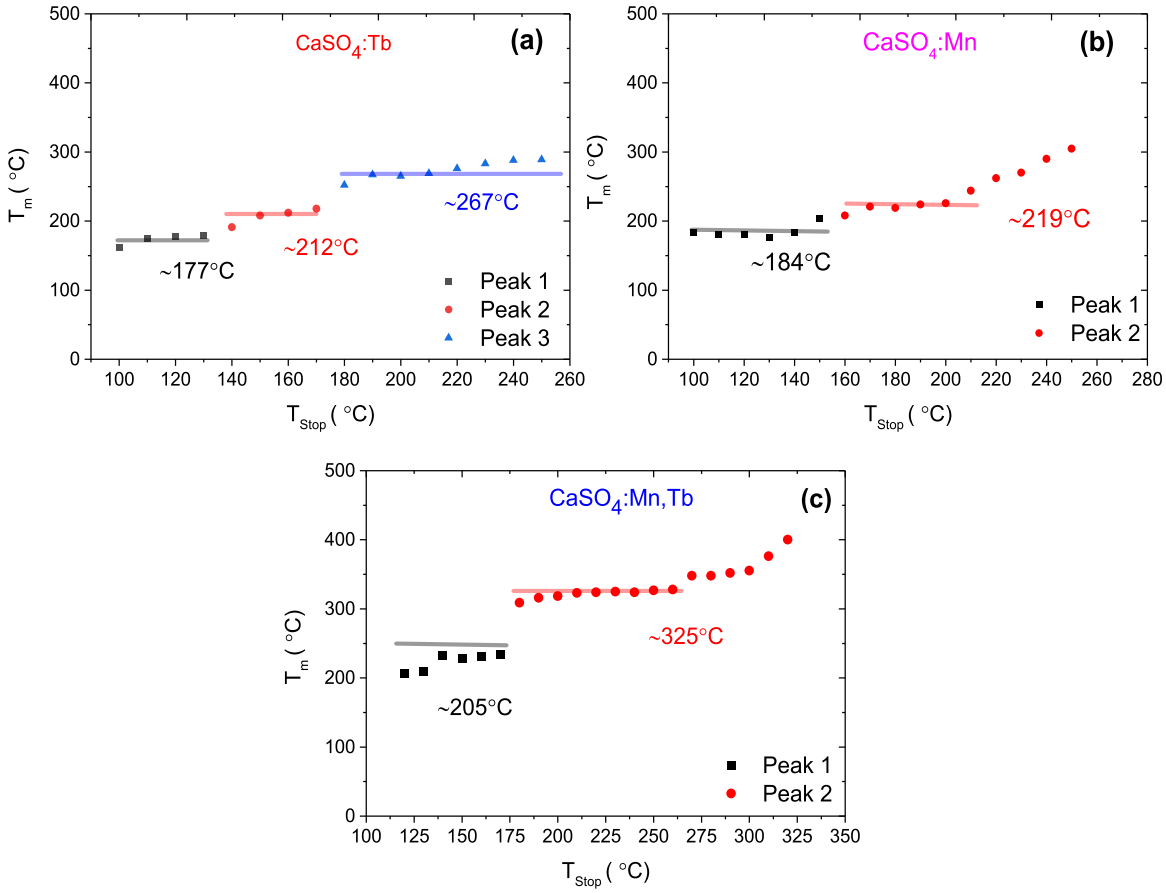

Fig. 7. $T_m \times T_{stop}$ curves obtained under various preheating temperatures (T_{stop}) for (a) $CaSO_4$:Tb, (b) $CaSO_4$:Mn, and (c) $CaSO_4$:Mn,Tb samples irradiated with 1 Gy of beta radiation.

peaks centered at 179 and 212 °C, along with a low-intensity peak centered at 267 °C. The TL emission of $CaSO_4$:Mn is characterized by the overlap of two peaks centered at 185 and 220 °C. The $CaSO_4$:Mn,Tb sample also showed a TL emission curve with two peaks but at higher temperatures compared to the mono-doped compound, with the first peak at 205 °C and the second at 325 °C.

3.6. Optically stimulated luminescence studies

3.6.1. OSL decay curves

Fig. 13 shows a typical OSL exponential decay curve for samples exposed to 1 Gy of beta radiation. For this analysis, the samples were optically stimulated using continuous blue light with an integration time of 40 s. For all samples, the OSL signal follows a trend of exponential decay as the traps are emptied. In particular, $CaSO_4$:Mn shows the highest OSL intensity, followed by $CaSO_4$:Mn,Tb, and then $CaSO_4$:Tb. This pattern mirrors the observed behavior in the TL emission of these phosphors.

3.6.2. OSL sensitivity

The OSL sensitivity analysis compares the OSL signal of the $CaSO_4$:Tb, $CaSO_4$:Mn, and $CaSO_4$:Mn,Tb samples with that of established dosimeters (Al_2O_3:C, the TLD-200, the TLD-400, and the TLD-900). Fig. 14a illustrates the OSL sensitivity, quantified by the integrals of the OSL decay curves per unit mass per unit of absorbed dose (OSL mg^{-1} Gy^{-1}). The materials were irradiated with 1 Gy of beta radiation. The results showed that the samples prepared in this study exhibited significantly higher sensitivity compared to the TLD-900, the TLD-400, and the TLD-200. However, Al_2O_3:C demonstrated greater sensitivity. The area under the OSL decay curve represents the total amount of light emitted over time. Although $CaSO_4$:Mn and $CaSO_4$:Mn,Tb exhibit higher OSL intensity, their luminescence decays faster because of a higher fast decay component, resulting in a smaller total area under the decay curve compared to $CaSO_4$:Tb. Fig. 14b shows the OSL decay curves for the studied samples and commercial TLD dosimeters.

3.6.3. OSL dose-response

In Fig. 15, the behaviors of the integral curves of the OSL as a function of the radiation dose for $CaSO_4$:Tb, $CaSO_4$:Mn, and $CaSO_4$:Mn,Tb phosphors exposed to beta radiation are illustrated. A linear relationship is observed in the range of 0.1–100 Gy. Linear fittings of the OSL response in the studied dose range showed linear correlation coefficients of 0.975 for $CaSO_4$:Tb, 0.991 for $CaSO_4$:Mn, and 0.994 for $CaSO_4$:Mn,Tb.

3.6.4. OSL fading

The investigation was extended to assess the OSL fading response of $CaSO_4$:Tb, $CaSO_4$:Mn, and $CaSO_4$:Mn,Tb samples after irradiation to a dose of 1 Gy ($^{90}Sr+^{90}Y$). Measurements were made immediately after irradiation and following a 30-day storage period at a temperature of 24 °C under constant environmental conditions, with the samples shielded from light. The results of this investigation are presented in Table 1.

Relative to the pellets evaluated immediately after irradiation, the OSL signal exhibited a 50% reduction for $CaSO_4$:Tb and a 60% reduction for $CaSO_4$:Mn after 30 days. While this fading was noticeable, it was comparatively less than that observed in the TL signal, as discussed in Section 3.5.3. Specifically, the samples co-doped with manganese and

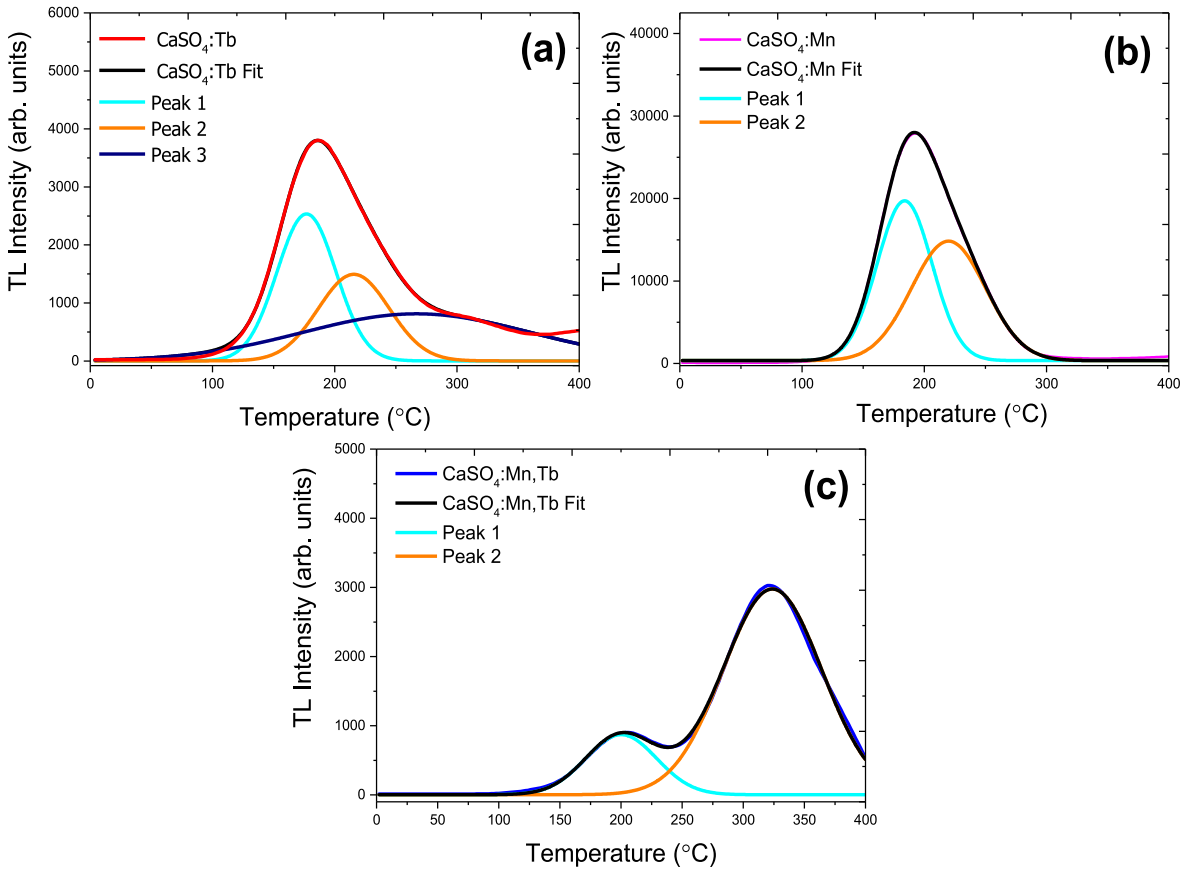

Fig. 8. TL glow curve deconvolution of (a) $CaSO_4$:Tb, (b) $CaSO_4$:Mn, and (c) $CaSO_4$:Mn,Tb samples irradiated with 1 Gy of beta radiation.

Table 1
OSL Responses of the $CaSO_4$:Tb, $CaSO_4$:Mn, and $CaSO_4$:Mn,Tb samples immediately after irradiation to a dose of 1 Gy ($^{90}Sr+^{90}Y$) and after a 30-day storage period.

Sample	Immediate OSL response (arb. units)	OSL response after 30 days (arb. units)	Luminescent signal (%)	OSL fading (%)
$CaSO_4$:Tb	$(1.01 \pm 0.01) \times 10^5$	$(5.09 \pm 0.21) \times 10^4$	50	50
$CaSO_4$:Mn	$(1.07 \pm 0.06) \times 10^5$	$(4.30 \pm 0.13) \times 10^4$	40	60
$CaSO_4$:Mn,Tb	$(6.07 \pm 0.20) \times 10^4$	$(5.49 \pm 0.47) \times 10^4$	90	10

terbium exhibited less intense OSL fading compared to TL fading. The OSL fading of $CaSO_4$:Mn,Tb was 9.6%, which is close to the observed TL fading of 10%. In comparison with recently published results on $CaSO_4$:Dy (Gasparian et al., 2022), which showed a significant OSL fading of 50% one day after irradiation, the findings of this study highlight the potential application of the produced dosimeters as effective OSL detectors for radiation dosimetry.

3.5.2. TL reproducibility, response, and sensitivity

Fig. 9 shows the variation of the TL response (area under the curve) of the pellets over five cycles comprising irradiation to a dose of 1 Gy, readout, and subsequent thermal treatment. Each data point represents the mean TL emission of 5 pellets and the bars represent their standard deviation. It is observed that the response of all samples after each cycle was similar, with variations of less than 8%. Therefore, it can be said that the TL signal of the produced samples is reproducible.

To evaluate the linearity of the TL response with dose, pellets were

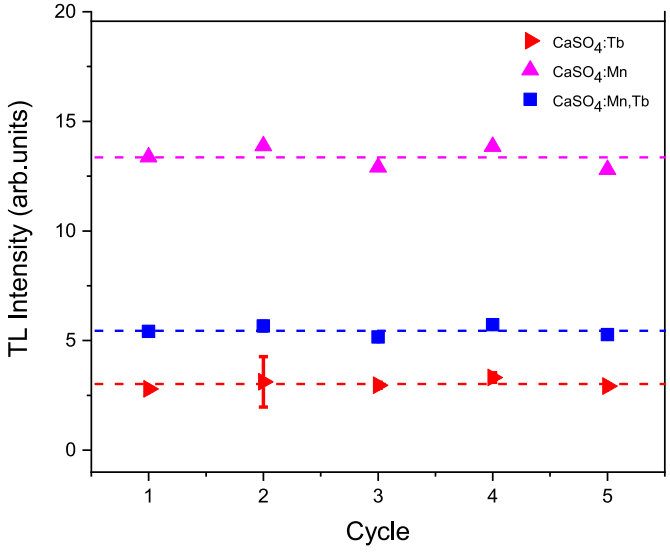

Fig. 9. TL response of $CaSO_4$:Tb, $CaSO_4$:Mn, and $CaSO_4$:Mn,Tb samples after each cycle comprising irradiation to a dose of 1 Gy, readout, and subsequent thermal treatment. The dashed lines represent the average TL response after 5 cycles.

irradiated at increasing doses from 0.169 to 100 Gy. The dose-response curve is shown in Fig. 10, with TL signal values determined by integrating the area under the emission curve. The pellets of the five phosphors exhibit a linear relationship between TL intensity and absorbed dose over the dose range studied. Linear fits, with correlation coefficients of 0.986 for $CaSO_4$:Tb, 0.993 for $CaSO_4$:Mn, and 0.989 for

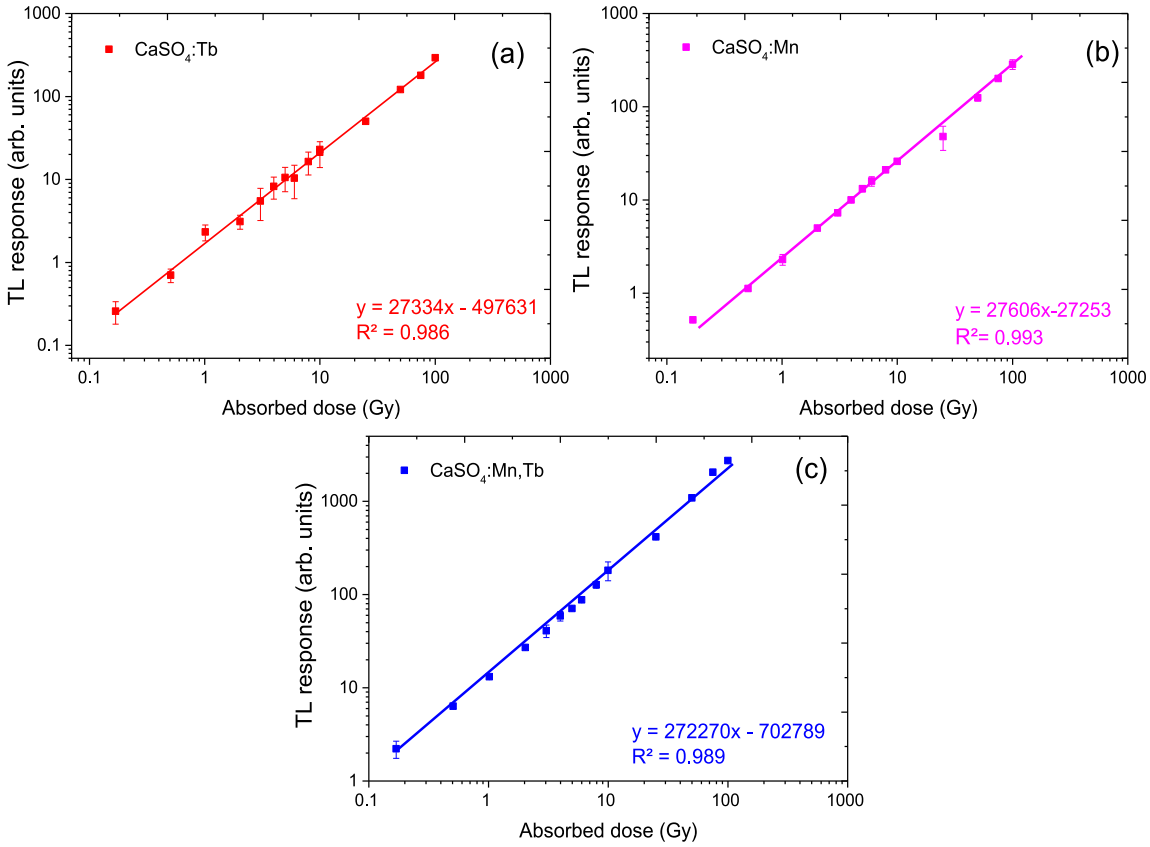

Fig. 10. TL Response of (a) $CaSO_4$:Tb, (b) $CaSO_4$:Mn, and (c) $CaSO_4$:Mn,Tb as a function of absorbed dose of beta radiation. The solid lines depict linear fits to the experimental data points.

$CaSO_4$:Mn,Tb, confirm the linearity of the dose-response curve.

The TL sensitivity analysis compares the TL signal of the $CaSO_4$:Tb, $CaSO_4$:Mn, and $CaSO_4$:Mn,Tb samples with that of established dosimeters (the TLD-100, the TLD-200, the TLD-400, and the TLD-900). Fig. 11a shows the TL sensitivity, quantified by the TL signal intensity per unit mass per unit of absorbed dose (TL mg^{-1} Gy^{-1}). The materials were irradiated with 1 Gy of beta radiation. The results showed that $CaSO_4$:Mn pellets exhibited significantly higher sensitivity compared to the TLD-400, the TLD-200, $CaSO_4$:Tb, $CaSO_4$:Mn,Tb, and the TLD-900. In other words, the $CaSO_4$:Mn pellets exhibited significantly higher TL sensitivity than all the other dosimeters tested, except the TLD-100 dosimeter. However, it is important to note that 50% of the pellets mass is Teflon and that this amount of Teflon does not significantly affect the luminescence signal of these dosimeters. Therefore, the results show that the materials proposed in this study are competitive from a dosimetric point of view. Fig. 11b shows typical TL emission curves for the samples and commercial dosimeters, demonstrating the significant potential of $CaSO_4$:Mn, $CaSO_4$:Tb, and $CaSO_4$:Mn,Tb for use in radiation dosimetry.

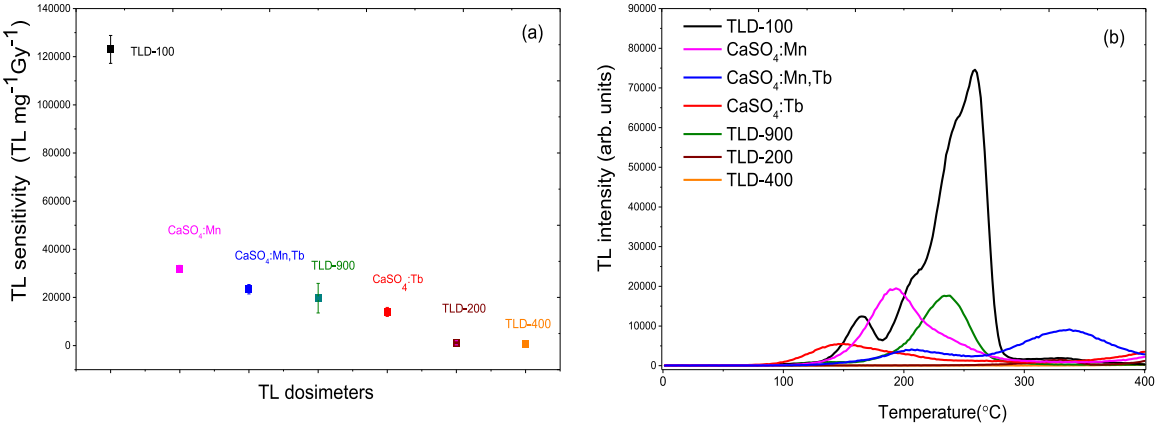

Fig. 11. (a) TL sensitivity of $CaSO_4$:Tb, $CaSO_4$:Mn, $CaSO_4$:Mn,Tb samples and commercial dosimeters irradiated with 1 Gy of beta radiation and (b) TL emission curves of $CaSO_4$:Tb, $CaSO_4$:Mn, $CaSO_4$:Mn,Tb samples and commercial dosimeters after irradiation.

3.5.3. Fading

To investigate the fading behavior of the TL signal of the $CaSO_4$:Tb and $CaSO_4$:Mn samples, their emission curves were read at intervals of 1, 7, 15, and 30 days after exposure to 1 Gy of radiation ($^{90}Sr+^{90}Y$). The samples were stored at room temperature (~23 °C) and shielded from light. The results are shown in Fig. 12a.

For $CaSO_4$:Tb, the emission curve showed a fading of 60% from its original value after irradiation. In the same period, $CaSO_4$:Mn samples showed a significant reduction of 75% in their TL signal. The preparation method of $CaSO_4$:Mn by slow evaporation resulted in a significant reduction of fading compared to other reports in the literature. In contrast to Bahl et al. (2017), who reported a significant loss of TL intensity (40%–85%) in the first 3 days after irradiation, our study showed a shift in the emission curve, with peak appearing at 190 °C. This discrepancy with previous work, where TL peaks were in the range of 100–140 °C (Medlin, 1961; Menon et al., 2005), suggests the presence of deeper traps in our studied samples.

The fading analysis of $CaSO_4$:Mn,Tb Involved comparing the TL emission curves of two groups of samples irradiated to a dose of 1 Gy, as shown in Fig. 12b. In the first group, TL was measured immediately after irradiation, while in the second group TL was measured after 30 days, with the samples stored under stable conditions at 24 °C during this period. The TL emission curves of the pellets evaluated after 30 days showed a 17% reduction in their original intensity. In particular, the TL peak above 250 °C showed relatively little fading after 30 days, with only a 10% reduction from the TL emission measured immediately after irradiation. Conversely, the peak below 250 °C experienced a significant reduction in intensity over the same period. This observation suggests that shallow traps are more easily released by thermal stimulation than traps with higher activation energies. From a dosimetric point of view, the second TL peak is more suitable than the first, as it occurs in a higher temperature range and fades less after irradiation. This result for $CaSO_4$:Mn,Tb suggests that co-doping with Mn and Tb contributes to the reduction of fading.

4. Conclusion

In this investigation, we conducted a detailed comparison of the luminescent properties of $CaSO_4$:Tb, $CaSO_4$:Mn, and $CaSO_4$:Mn,Tb crystals prepared by an adapted slow evaporation route. The XRD analyses confirmed the efficient synthesis of these crystals. The results obtained from the PL and RL analyses not only confirmed the presence of Tb^{3+} and Mn^{2+} ions in the crystal matrices, underscoring the successful generation of structural defects but also demonstrated the potential for their effective application. In addition, SEM images of the prepared pellets revealed essential and critical properties for dosimetric applications, such as homogeneity, a cohesive surface, and low porosity.

TL analyses revealed distinct emission curves for each crystal variant. $CaSO_4$:Mn exhibited overlapping TL peaks at 184 and 219 °C. Notably, even after 30 days, the TL fading was significantly lower than the reported values for alternative synthesis methods, highlighting the stability of the slow evaporation route. $CaSO_4$:Tb exhibited three TL peaks centered at 180, 210, and 270 °C; however, this sample faded by 60% after 30 days. The incorporation of Tb as a co-dopant in $CaSO_4$:Mn resulted in a TL curve with peaks at 205 and 325 °C, with a TL fade of 17 % after 30 days. Importantly, the fading of co-doped samples was found to be lower compared to mono-doped samples, reinforcing the

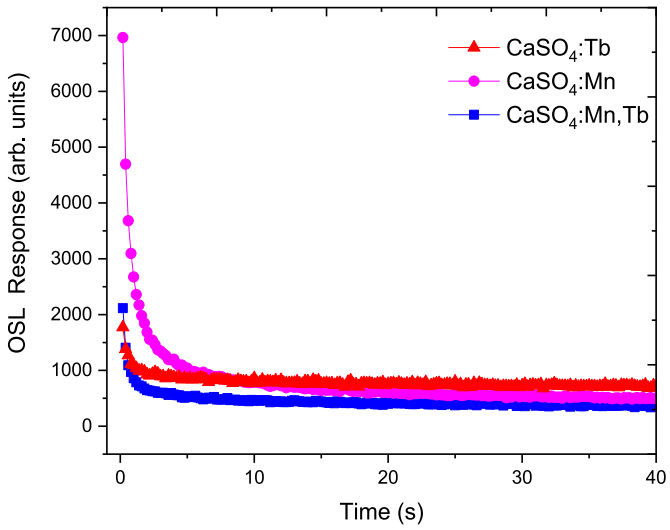

Fig. 13. OSL decay curve of $CaSO_4$:Tb, $CaSO_4$:Mn, and $CaSO_4$:Mn,Tb samples, irradiated with 1Gy of $^{90}Sr+^{90}Y$.

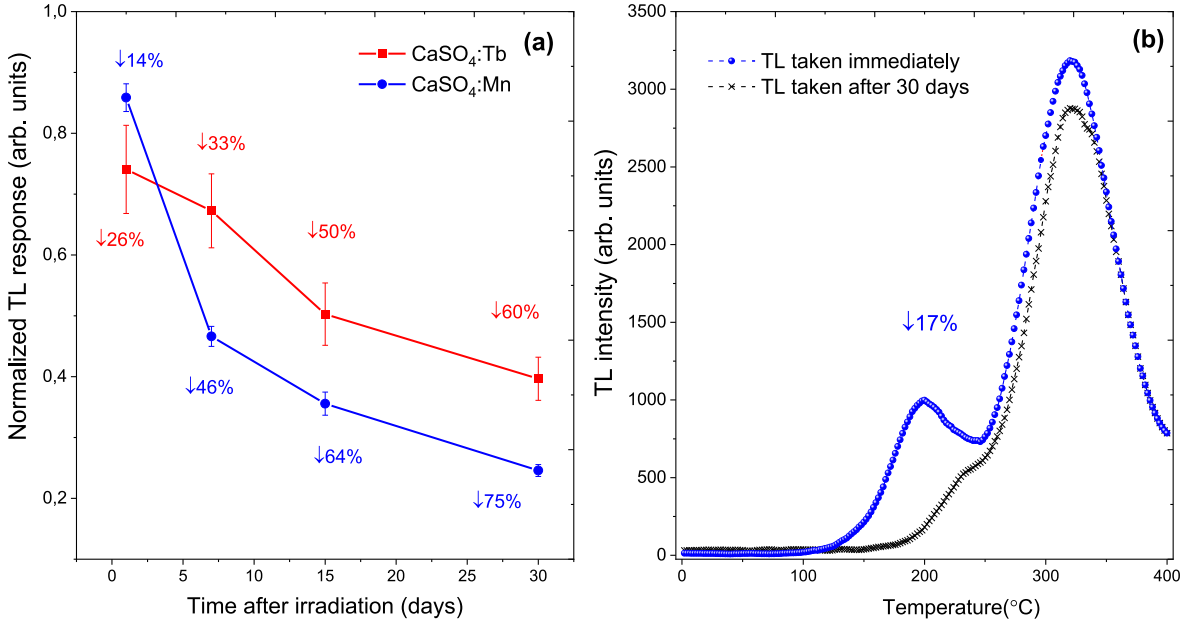

Fig. 12. (a) The normalized TL response of $CaSO_4$:Tb and $CaSO_4$:Mn,Tb samples plotted against the percentage of fading for different storage periods after irradiation to a dose of 1 Gy ($^{90}Sr+^{90}Y$) and (b) TL emission for $CaSO_4$:Mn,Tb samples irradiated to a dose of 1 Gy, read immediately after irradiation and after 30 days.

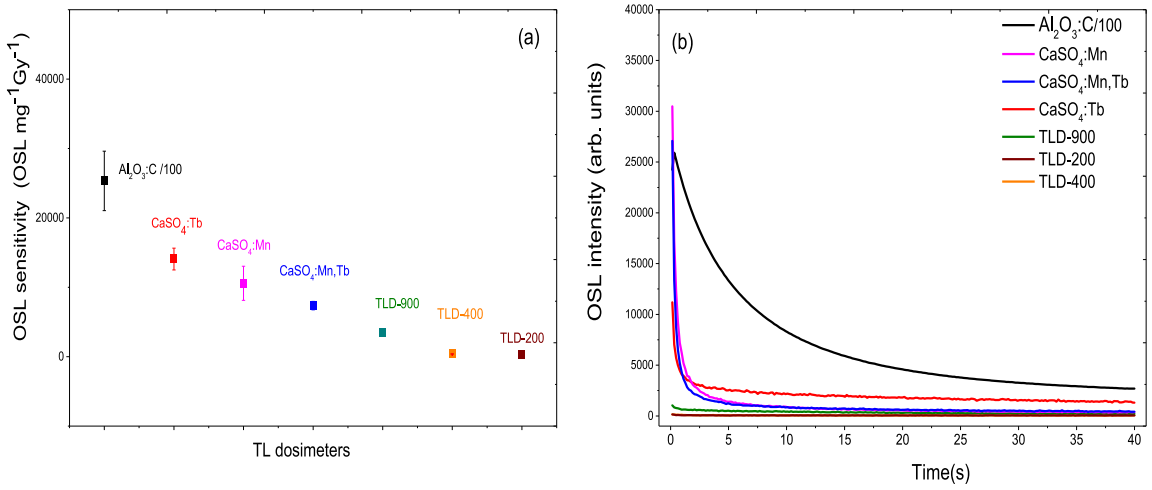

Fig. 14. (a) OSL sensitivity of the $CaSO_4$:Tb, $CaSO_4$:Mn, and $CaSO_4$:Mn,Tb samples compared to established dosimeters (Al_2O_3:C, the TLD-200, the TLD-400, and the TLD-900) and (b) OSL decay curves for the samples and commercial TLD dosimeters. Note that the OSL intensity of Al_2O_3 is divided by 100.

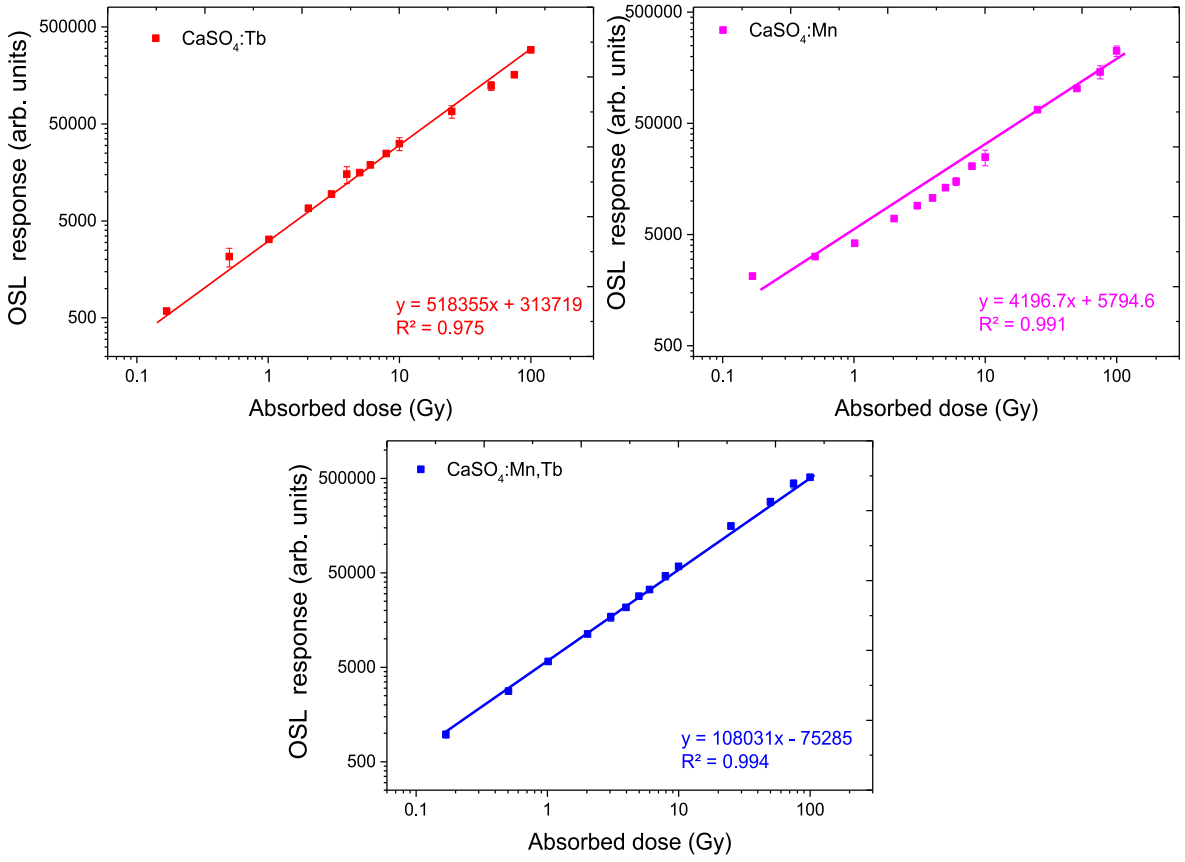

Fig. 15. OSL response of $CaSO_4$:Tb, $CaSO_4$:Mn, and $CaSO_4$:Mn,Tb samples as a function of absorbed dose after $^{90}Sr+^{90}Y$ irradiation (0.1–100 Gy). The solid lines depict linear fits to the experimental data.

advantageous properties of the co-doping approach.

Comparative TL/OSL analysis with commercial dosimeters revealed that the materials proposed are dosimetrically competitive, as only TLD-100 and Al_2O_3:C showed a slightly higher sensitivity than synthesized ones. All samples produced suitable OSL curves, with $CaSO_4$:Mn showing the highest intensity. The fading of the samples' TL signal 30 days after irradiation was 49% for $CaSO_4$:Tb, 60% for $CaSO_4$:Mn, and 9.6% for $CaSO_4$:Mn,Tb. The pellets exhibited suitable luminescent properties and dosimetric properties, including linear luminescent response ranging from a few mGy to 100 Gy and reproducibility of both OSL and TL signals.

CRediT authorship contribution statement

Anderson M.B. Silva: Writing – original draft, Methodology, Investigation, Formal analysis, Data curation, Conceptualization.

Daniel S. Rodrigues: Investigation. **Beatriz D.O. Guedes:** Investigation. **Iury S. Silveira:** Investigation. **Patrícia L. Antonio:** Investigation. **Danilo O. Junot:** Writing – review & editing, Investigation, Formal analysis, Data curation. **Linda V.E. Caldas:** Writing – review & editing, Funding acquisition, Formal analysis, Conceptualization. **Divanizia N. Souza:** Writing – review & editing, Validation, Supervision, Project administration, Funding acquisition.

Declaration of competing interest

The authors declare the following financial interests/personal relationships which may be considered as potential competing interests. Divanizia N. Souza reports financial support was provided by National Council for Scientific and Technological Development. Anderson M. B. Silva reports financial support was provided by Brazilian Nuclear Energy Commission. If there are other authors, they declare that they have no known competing financial interests or personal relationships that could have appeared to influence the work reported in this paper.

Data availability

Data will be made available on request.

Acknowledgments

The authors thank the Brazilian agencies Comissão Nacional de Energia Nuclear - CNEN (Project 1342.005453/2023–19), Conselho Nacional de Desenvolvimento Científico e Tecnológico - CNPq (Projects: 07493/2021-2, 405536/2023–2, 406761/2022-1, and 305142/2021–6, Fundação de Amparo à Pesquisa do Estado de São Paulo - FAPESP (Project: (2023/04859-8,and 2018/05982–0) and MultiLab (Multi-User Physics Laboratories) and CLQM (Center of Multi-users Chemistry Laboratories) from Federal University of Sergipe for the analysis support.

References

Antonov-Romanovskii, V.V., Keirum-Markus, I.F., Poroshina, M.S., Trapeznikova, Z.A., 1955. IR stimulable phosphors, Conference of the academy of sciences of the USSR on the peaceful uses of. Atom. Energy 239–250. Moscow.

Bahl, S., Kumar, V., Bihari, R.R., Kumar, P., 2017. Investigations of OSL properties of $CaSO_4$:Mn phosphor exposed to gamma and beta radiations. J. Lumin. 181, 36–43. https://doi.org/10.1016/j.jlumin.2016.09.004.

Bakr, M., Portakal Ucar, Z.G., Yuksel, M., Kaynar, U.H., Ayvacikli, M., Benourdja, S., Canimoglu, A., Topaksu, M., Hammoudeh, A., Can, N., 2020. Thermoluminescence properties of beta particle irradiated $Ca_3Al_2O_6$ phosphor relative to environmental dosimetry. J. Lumin. 227, 117565 https://doi.org/10.1016/j.jlumin.2020.117565.

Chen, R., McKeever, S.W.S., 1997. Theory of Thermoluminescence and Related Phenomena. World Scientific, New Jersey.

Daniels, F., Boyd, C.A., Saunders, D.F., 1953. Thermoluminescence as a research tool. Sci. 117, 343–349.

Dasa, R., Gupta, K., Jana, K., Nayak, A., Ghosh, U.C., 2016. Preparation, characterization and dielectric, ac conductivity with electrochemical behavior of strontium zirconate. Adv. Mater. Lett. 7, 646–651. https://doi.org/10.5185/amlett.2016.6294.

Dexter, D.L., 1953. A theory of sensitized luminescence in solids. J. Chem. Phys. 21, 836–850. https://doi.org/10.1063/1.1699044.

Doull, B.A., Oliveira, L.C., Wang, D.Y., Milliken, E.D., Yukihara, E.G., 2014. Thermoluminescent properties of lithium borate, magnesium borate and calcium sulfate developed for temperature sensing. J. Lumin. 146, 408–417. https://doi.org/10.1016/j.jlumin.2013.10.022.

Fernández, S.D.S., García-Salcedo, R., Mendoza, J.G., Sánchez-Guzmán, D., Rodríguez, G. R., Gaona, E., Montalvo, T.R., 2016. Thermoluminescent characteristics of LiF: Mg, Cu, P and $CaSO_4$: Dy for low dose measurement. App. Radiat. Isot. 111, 50–55. https://doi.org/10.1016/j.apradiso.2016.02.011.

Gasparian, P.B.R., Malthez, A.L.M.C., Yoshimura, E.M., Umisedo, N.K., Campos, L.L., 2022. Study of the dosimetric properties of $CaSO_4$: Dy using OSL technique. J. Instrum. 17, 4022. https://doi.org/10.1088/1748-0221/17/04/P04022.

Guckan, V., Altunal, V., Nur, N., Depci, T., Ozdemir, A., Kurt, K., Yu, Y., Yegingil, I., Yegingil, Z., 2017. Studying CaSO4:Eu as an OSL phosphor. Nucl. Instrum. Methods Phys. Res. B: Beam Interact. Mater. At. 407, 145–154. https://doi.org/10.1016/j.nimb.2017.06.010.

Guckan, V., Ozdemir, A., Altunal, V., Yegingil, I., Yegingil, Z., 2019. Studies of blue light induced phototransferred thermoluminescence in $CaSO_4$:Mg. Nucl. Instrum. Methods Phys. Res. B: Beam Interact. Mater. At. 448, 31–38. https://doi.org/10.1016/j.nimb.2019.03.058.

Guckan, V., Bereket, S., Altunal, V., Abusaid, W., Yegingil, Z., 2023. Luminescence properties of Tb and Eu activated $CaSO_4$ phosphor. Radiat. Phys. Chem. 203, 110620 https://doi.org/10.1016/j.radphyschem.2022.110620.

Haninger, T., Hodlmoser, H., Figel, M., Konig-Meier, D., Henniger, J., Sommer, M., Jahn, A., Ledtermann, G., Eber, R., 2016. Properties of the BeOSL dosimetry system in the framework of a large-scale personal monitoring service. Radiat. Prot. Dosim. 170, 269–273. https://doi.org/10.1093/rpd/ncv425.

Hao, Z., Zhang, J., Zhang, X., Lu, S., Wang, X., 2009. Blue-green-emitting phosphor $CaSc_2O_4$: Tb^{3+}: tunable luminescence manipulated by cross-relaxation. J. Electrochem. Soc. 156, 193. https://doi.org/10.1149/1.3060382.

Hou, D., Liu, C., Kuang, X., Liang, H., 2012. Enhanced emission of Mn^{2+} via Ce^{3+}→Mn^{2+} energy transfer in α-$Sr_2P_2O_7$. Opt Express 20, 28969–28980. https://doi.org/10.1364/OE.20.028969.

Junot, D.O., Santos, A.G., Antonio, P.L., Rezende, M.V., Souza, D.N., Caldas, L.V.E., 2019. Dosimetric and optical properties of $CaSO_4$:Tm and $CaSO_4$: Tm, Ag crystals produced by a slow evaporation route. J. Lumin. 210, 58–65. https://doi.org/10.1016/j.jlumin.2019.02.005.

Junot, D.O., Souza, D.N., Caldas, L.V.E., 2020. TL/OSL signal of $CaSO_4$: Eu, Ag samples produced by variations of the slow evaporation route. Radiat. Meas. 135, 106334 https://doi.org/10.1016/j.radmeas.2020.106334.

Junot, D.O., Barros, J.P., Caldas, L.V.E., Souza, D.N., 2016. Thermoluminescent analysis of $CaSO_4$:Tb,Eu crystal powder for dosimetric purposes. Radiat. Meas. 90, 228–232. https://doi.org/10.1016/j.radmeas.2016.01.020.

Junot, D.O., Santos, M.A.C., Antonio, P.L., Caldas, L.V.E., Souza, D.N., 2014. Feasibility study of $CaSO_4$:Eu, $CaSO_4$:Eu,Ag and $CaSO_4$:Eu,Ag(NP) as thermoluminescent dosimeters. Radiat. Meas. 71, 99–103. https://doi.org/10.1016/j.radmeas.2014.05.022.

Junot, D.O., Vasconcelos, D.F., Chagas, M.A.P., Santos, M.A.C., Caldas, L.V.E., Souza, D. N., 2011. Silver addition in $CaSO_4$:Eu, TL and TSEE properties. Radiat. Meas. 46, 1500–1502. https://doi.org/10.1016/j.radmeas.2011.06.049.

Kadari, A., Mahi, K., Mostefa, R., Badaoui, M., Mameche, A., Kadri, D., 2016. Optical and structural properties of Mn doped $CaSO_4$ powders synthesized by sol-gel process. J. Alloys Compd. 688, 32–36. https://doi.org/10.1016/j.jallcom.2016.07.040.

Kása, I., Chobola, R., Mell, P., Szakács, S., Kerekes, A., 2007. Preparation and investigation of thermoluminescence properties of $CaSO_4$:Tm,Cu. Radiat. Prot. Dosim. 123, 32–35. https://doi.org/10.1093/rpd/ncl088.

Khan, Z.S., Ingale, N.B., Omanwar, S.K., 2015. Thermoluminescence studies of terbium doped calcium sulfate phosphor. Int. J. Lumin. Appl. 5, 471–474.

Lakshmanan, A.R., 1999. Photoluminescence and thermostimulated luminescence processes in rare-earth-doped $CaSO_4$ phosphors. Prog. Mater. Sci. 44, 1–187. https://doi.org/10.1016/S0079-6425(99)00003-1.

Li, M., Wang, L., Ran, W., Deng, Z., Shi, J., Ren, C., 2017. Tunable luminesce nce in $Sr_2MgSi_2O_7$: Tb^{3+}, Eu^{3+} phosphors based on energy transfer. Mater 10, 227. https://doi.org/10.3390/ma10030227.

Luchechko, A., Zhydachevskyy, Y., Ubizskii, S., Kravets, O., Popov, A.I., Rogulis, U., Suchocki, A., 2019. Afterglow, TL and OSL properties of Mn^{2+} doped $ZnGa_2O_4$ phosphor. Sci. Rep. 9, 1–8. https://doi.org/10.1038/s41598-019-45869-7.

Marzougui, H., Hassen-Chehimi, D.B., 2019. Study of structural and optical properties of Nd^{3+} doped K_2Mg_2 (SO_4) ^{3} langbeinite salts. Inorg. Chem. Commun. 104, 201–206. https://doi.org/10.1016/j.inoche.2019.04.009.

McKeever, S.W.S., 1988. Thermoluminescence of Solids. Cambridge University Press, Cambridge.

McKeever, S.W.S., Moscovitch, M., Townsend, P.D., 1995. Thermoluminescence Dosimetry Materials: Properties and Uses. Nuclear Technology Pub, Ashford, UK.

McKeever, S.W., 2022. A Course in Luminescence Measurements and Analyses for Radiation Dosimetry. Wiley.

Medlin, W.L., 1961. Thermoluminescence in anhydrite. J Phys Chem Solids 18, 238–252.

Menon, S.N., Sanaye, S.S., Dhabekar, B.S., Kumar, R., Bhatt, B.C., 2005. Role of Mn as a co-dopant in $CaSO_4$: Mn, Pr TL phosphor. Radiat. Meas. 39, 111–114. https://doi.org/10.1016/j.radmeas.2004.06.004.

Nakauchi, D., Okada, G., Koshimizu, M., Yanagida, T., 2016. Storage luminescence and scintillation properties of Eu-doped $SrAl_2O_4$ crystals. J. Lumin. 176, 342–346. https://doi.org/10.1016/j.jlumin.2016.04.008.

Pradhan, A.S., Lee, J.I., Kim, J.L., 2008. Recent developments of optically stimulated luminescence materials and techniques for radiation dosimetry and clinical applications. J. Med. Phys. 33, 85–99. https://doi.org/10.4103/0971-6203.42748.

Rani, R.S., Lakshmanan, A.R., Sivakumar, V., Venkatasamy, R., Annalakshmi, O., Jose, M.T., Marimuthu, K.N., 2015. Redox and charge transfer processes and luminescence in $CaSO_4$:Zn,Mn. Radiat. Meas. 76, 1350–4487. https://doi.org/10.1016/j.radmeas.2015.03.001.

Silva, A.M.B., Silveira, W.S., Matos, T.S., Junot, D.O., Rezende, M.V., Souza, D.N., 2021. Effect of terbium and silver co-doping on the enhancement of photoluminescence in $CaSO_4$ phosphors. Opt. Mater. 111, 110717 https://doi.org/10.1016/j.optmat.2020.110717.

Silva, A.M.B., Souza, L.F., Antonio, P.L., Junot, D.O., Caldas, L.V.E., Souza, D.N., 2022. Effects of manganese and terbium on the dosimetric properties of $CaSO_4$. Radiat. Phys. Chem. 198, 110207 https://doi.org/10.1016/j.radphyschem.2022.110207.

Silva, A.M.B., Junot, D.O., Caldas, L.V.E., Souza, D.N., 2020. Structural, optical and dosimetric characterization of $CaSO_4$:Tb, $CaSO_4$:Tb,Ag and $CaSO_4$:Tb,Ag(NP). J. Lumin. 224, 117286 https://doi.org/10.1016/j.jlumin.2020.117286.

Silva, A.M.B., Rodrigues, D.S., Antonio, P.L., Junot, D.O., Caldas, L.V., Souza, D.N., 2023. Investigation of dosimetric properties of $CaSO_4$:Mn phosphor prepared using slow evaporation route. Appl. Radiat. Isot. 199, 110874 https://doi.org/10.1016/j.apradiso.2023.110874.

Totsuka, D., Yanagida, T., Fukuda, K., Kawaguchi, N., Fujimoto, Y., Pejchal, J., Yoshikawa, A., 2011. Performance test of Si PIN photodiode line scanner for thermal

neutron detection. Nucl. Instr. Meth. Phys. Res. 659, 399. https://doi.org/10.1016/j.nima.2011.08.014.

Van der Kolk, E., Dorenbos, P., Vink, A.P., Perego, R.C., Van Eijk, C.W.E., Lakshmanan, A.R., 2001. Vacuum ultraviolet excitation and emission properties of Pr^{3+} and Ce^{3+} in MSO_4 (M= Ba, Sr, and Ca) and predicting quantum splitting by Pr^{3+} in oxides and fluorides. Phys. Rev. B 64, 195129. https://doi.org/10.1103/PhysRevB.64.195129.

Watanabe, K., 1951. Properties of $CaSO_4$:Mn phosphor under vacuum ultraviolet excitation. Phys. Rev. 83, 785–791. 1. https://doi.org/10.1103/PhysRev.83.78.

Yamashita, T., Sakai, K., Kitamura, S., 1970. Calcium sulfate activated by lead and manganese for thermoluminescence dosimetry. J. Nucl. Sci. (Seoul) 7, 105–110. https://doi.org/10.1080/18811248.1970.9734651.

Yanagida, T., Yoshikawa, A., Yokota, Y., Kamada, K., Usuki, Y., Yamamoto, S., Ohuchi, N., 2010. Development of Pr: LuAG scintillator array and assembly for positron emission mammography. IEEE Trans. Nucl. Sci. 57, 1492–1495. https://doi.org/10.1109/TNS.2009.2032265.

Yasmin, S., Khandaker, M.U., Rozaila, Z.S., Rashid, M.A., Bradley, D.A., Sani, S.A., 2020. Thermoluminescence features of commercial glass and retrospective accident dosimetry. Radiat. Phys. Chem. 168, 108528 https://doi.org/10.1016/j.radphyschem.2019.108528.

You, H., Song, Y., Jia, G., Hong, G., 2008. Energy transfer from Tb^{3+} to Mn^{2+} in LaMgAl11O19:Tb,Mn phosphors. Opt. Mater. 31 (2), 342–345. https://doi.org/10.1016/j.optmat.2008.05.005.

Yukihara, E.G., Coleman, A.C., Bastani, S., Gustafson, T., Talghader, J.J., Daniels, A., Svingala, F.R., 2015. Particle temperature measurements in closed chamber detonations using thermoluminescence from $Li_2B_4O_7$: Ag,Cu, MgB_4O_7:Dy,Li and $CaSO_4$:Ce,Tb. J. Lumin. 165, 145–152. https://doi.org/10.1016/j.jlumin.2015.04.031.

Yukihara, E.G., Coleman, A.C., Doull, B.A., 2014. Passive temperature sensing using thermoluminescence: laboratory tests using $Li_2B_4O_7$:Cu,Ag, MgB_4O_7:Dy,Li and $CaSO_4$:Ce,Tb. J. Lumin. 146, 515–526. https://doi.org/10.1016/j.jlumin.2013.10.048.

Zahedifar, M., Mehrabi, M., Harooni, S., 2011. Synthesis of $CaSO_4$:Mn nanosheets with high thermoluminescence sensitivity. Appl. Radiat. Isot. 69, 1002–1006. https://doi.org/10.1016/j.apradiso.2011.01.036.